Charge Order and Negative Thermal Expansion in V2OPO4

OPEN ACCESS

Charge order and negative thermal expansion in V_2OPO_4

Elise Pachoud, James Cumby, Calum T. Lithgow, J. Paul Attfield*

Centre for Science at Extreme Conditions and School of Chemistry, University of Edinburgh, Edinburgh EH9 3FD, United Kingdom.

ABSTRACT: The semivalent oxyphosphate V_2OPO_4 is found to have long range V^{2+}/V^{3+} charge ordering up to 605 K where a monoclinic to tetragonal structural transition and a switch from positive to negative thermal expansion are observed. V-V bonding within orbital polymer chains is proposed as the key factor in the novel switch of thermal expansion behavior, as loss of V-V bonding enables transverse oxygen motions to dominate the thermal expansion at high temperatures. Ferrimagnetic order of V^{2+} spin up and V^{3+} spin down states is observed below a magnetic ordering transition at 164 K, and susceptibility measurements evidence local spin pairing correlations to higher temperatures.

INTRODUCTION

Negative thermal expansion (NTE), where the volume of a substance decreases upon heating, is an unusual property that is of fundamental interest and finds application in creating zero expansion materials [1]. There are two basic types of mechanism for NTE. Large-amplitude transverse vibrations or torsions can lead to NTE in insulating framework materials such as $Zr(WO_4)_2$ [2,3] or ScF_3 [4,5], and changes in band structure associated with electronic or magnetic transitions may result in NTE in metal alloys and ceramics, for example, colossal NTE effects associated with charge ordering in the perovskite $BiNiO_3$ [6]. We report here a novel mechanism where lattice thermal expansion switches from normal, positive behavior (PTE) to NTE driven by the loss of metal-metal bonding associated with charge ordering.

This study is part of an investigation of materials containing orbital molecules, directly bonded clusters of transition metal ions in orbitally-ordered solids [7]. Low valent vanadium oxides with short V-V distances are notable for forming large orbital molecules. $BaV_{10}O_{15}$ forms triangular V_3^{9+} clusters below a structural and semiconductor-insulator transition at 130 K [8,9,10], and the spinel AlV_2O_4 is reported to have heptameric V_7^{17+} orbital molecules below the charge order transition at 700 K [11].

We have explored the semivalent oxyphosphate V_2OPO_4 which was previously reported to have a tetragonal structure at room temperature (Figure 1a) consisting of a stacking along the c axis of non-intersecting chains of face-sharing $V^{2.5+}O_6$ octahedra, running alternatively parallel to a and b [12]. The intrachain V-V distance of 2.68 Å is very short so direct bonding interactions are expected. A structural transition was reported near 593 K but no details were given. In this paper we report the synthesis, structural and magnetic characterization of V_2OPO_4 over a wide temperature range, from 4 to 750 K. Separate charge and ferrimagnetic ordering transitions are found, and the former leads to the unusual switch from positive to negative thermal volume expansion that we attribute to the loss of V-V bonding in 'orbital polymer' chains.

EXPERIMENTAL SECTION

A polycrystalline sample of V_2OPO_4 was prepared by high temperature solid state reaction as previously reported by Glaum [6]. The precursor β-$VOPO_4$ was prepared by heating a stoichiometric mixture of NH_4VO_3 and $(NH_4)_2HPO_4$ at 600°C in flowing O_2 twice for 8 hours [13]. A stoichiometric mixture of β-$VOPO_4$ and V was thoroughly ground, pressed into pellets, and heated in an evacuated sealed silica tube. Good crystallinity and high product purity were obtained after three heating cycles at 1000 °C of ca. 30 hours each, with intermediate regrinding and pelletizing.

Phase purity of the product was checked by X-ray powder diffraction (XRD) using a Bruker D2 diffractometer with CuKα radiation and 5° - 70° 2θ range. High resolution synchrotron XRD data has been collected on the I11 diffractometer at the Diamond facility using the wavelength λ = 0.82582Å at 270, 180 and 140 K, and from 300 up to 750 K with λ = 0.825775 Å. For the high temperature experiment, the sample was loaded in a quartz capillary inside a glove bag filled with argon to prevent possible oxidation at high temperature. However, some decomposition or reaction of the product with the quartz was observed at temperatures above 750 K. Time of flight neutron powder diffraction (NPD) data were collected at 298 K and between 10 and 290 K in 20 K steps using a He cryostat on HRPD at the ISIS source. The sample was placed in an aluminum-framed slab can with vanadium windows. All the diffraction data were analyzed using Fullprof software [14].

Magnetic properties were measured in a Quantum Design SQUID magnetometer. Magnetization vs. temperature from 10 to 400 K in a field of 0.1 T, and vs. applied magnetic field from -5 to 5 T at 5, 140 and 160 K, were measured. Resistivity measurements were carried out with the 4 point probe method using a Quantum Design PPMS from 10 to 300 K and in a lab-made apparatus from 300 to 870 K; the sample was placed inside a vacuum furnace and connected to a Keithley 2010 multimeter while the temperature was measured at the sample holder.

Electronic structure calculations were performed using CASTEP (v17.2) [15] using inbuilt on-the-fly pseudopotentials. Plane-wave energy cut-off (700 eV) and k-point density (5×5×4 Monkhorst-Pack grid [16]) were both well-converged.

[Partial] density of states ([p]DOS) were produced using OptaDOS (v1.2) with the adaptive peak broadening method [17,18]. Calculations were performed within the appropriate primitive unit cell.

RESULTS AND DISCUSSION

Crystal structure at room temperature. High resolution neutron and synchrotron X-ray diffraction patterns of V_2OPO_4 at 298 K are not properly indexed with the reported tetragonal $I4_1/amd$ cell as splittings of some peaks are clearly visible as shown in Fig. 1. The peaks can be indexed using a monoclinic $C2/c$ supercell with a_M = 7.56825 Å b_M = 7.60013(7) Å, c_M = 7.21794(6) Å, β_M = 121.2751(5)°, similar to that of the iron analogue β-Fe_2OPO_4 where a partial $Fe^{2.4+}/Fe^{2.6+}$ charge ordering accompanying the monoclinic distortion below 410 K was reported [19]. Some anisotropic peak broadening was observed and was fitted using Stephens strain model [20], with S_{202} being the dominant parameter.

The relationship between the monoclinic and ideal (high temperature) tetragonal cells of V_2OPO_4 is shown in Fig. 1a. The transformation from monoclinic to tetragonal including origin shift is shown by matrix (1). For convenience we express the monoclinic cell in a pseudo-tetragonal metric, with 298 K parameters $a_T = b_T$ = 5.36282(2) Å, c_T = 12.3383(1) Å, α_T = 180° - β_T = 89.7584(5)°, γ_T = 89.7596(7)°. The proximities of the cell angles to 90° illustrate the small magnitude of the lattice distortion.

$$\begin{pmatrix} -0.5 & 0.5 & 1 & 0.5 \\ -0.5 & -0.5 & 0 & 1 \\ 0 & 0 & 2 & 0 \\ 0 & 0 & 0 & 1 \end{pmatrix} \quad (1)$$

The monoclinic distortion maintains uniform distances of 2.68 Å between neighboring V atoms in the chains, so there is no evidence for orbital dimerization as occurs below the Peierls transition in VO_2 [21]. Attempts to lower symmetry further generating inequivalent in-chain distances in the refinement did not lead to significant V-displacements or improved fits. The monoclinic distortion creates distinct V1 and V2 sites that alternate along the chains. The average V-O distances in the VO_6 octahedra differ significantly as 2.095 and 2.027 Å for V1 and V2. Interpolation of bond valence sums (BVS) [22] give respective values of +2.1 for V1 and +2.7 for V2, showing that V^{2+}/V^{3+} charge ordering is present in the monoclinic phase of V_2OPO_4.

Low temperature magnetic properties. Magnetic susceptibility measurements shown in Figure 2a reveal a magnetic ordering transition at T_C = 164 K to a ferro- or ferri- magnetic state, with a divergence between the zero field and field cooled data. Above the transition the inverse susceptibility is not linear and so does not follow standard Curie-Weiss behavior. However, the addition of a constant according to, χ = $C/(T-\theta) + \chi_0$, gives a very good fit to data at 170 - 400 K with fitting parameters θ = 165.6 K, χ_0 = 0.00136 emu.mol^{-1} and C = 0.322 emu.K.mol^{-1}. The latter value gives a paramagnetic moment of μ_{eff} = 1.61 μ_B per V_2OPO_4 unit, which is greatly reduced below the ideal value of 3.39 μ_B for uncoupled V^{2+} and V^{3+} spins. This and the large value of the constant term χ_0 show that strong short-range antiferromagnetic coupling of spins persists in the paramagnetic regime immediately above T_C.
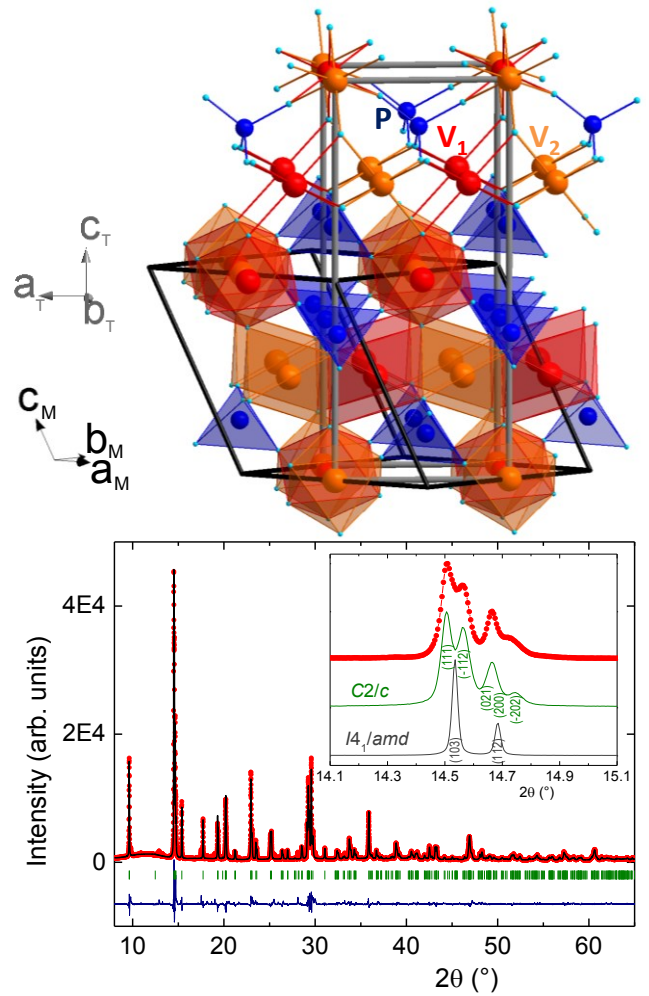

Figure 1. (a) Crystal structure of V_2OPO_4 showing axes and unit cells for the monoclinic $C2/c$ (in black) and the tetragonal $I4_1/amd$ (grey) symmetries. (b) Fit of the monoclinic structure to 298 K synchrotron XRD data. Inset shows the monoclinic splitting of the intense peaks near 14.5° with indexed simulations for $I4_1/amd$ and $C2/c$ cells.

Isothermal magnetization vs. magnetic field exhibit a hysteresis loop below T_C (Figure 2b). At 5 K, the saturated magnetization at 5 T is 0.6 μ_B per formula unit. V_2OPO_4 has a large coercive field of 0.8 T, characteristic of a moderately hard magnetic material with strong spin anisotropy.

The magnetic structure of V_2OPO_4 has been solved using the NPD patterns collected at 10 K on HRPD. Magnetic intensities appearing below T_C are superimposed on nuclear peaks and are indexed by the propagation vector (0 0 0). Representation analysis was performed using the BasIreps program from the Fullprof suite. Only one of the two possible magnetic representations (Table S3) gives a good fit to the prominent magnetic peak at $d \approx 3.8$ Å (Figure 3a). This corresponds to a ferromagnetic arrangement of spins within each sublattice, with V1 and V2 spins coupled antiparallel to each other so the overall magnetic order is ferrimagnetic. Temperature variations of the refined moments are shown in Figure 3b. The weak intensities of the magnetic peaks did not enable the spin directions within the monoclinic ac-plane to be determined uniquely from the magnetic fits, and they were constrained to lie parallel to the pseudo-tetragonal c_T axis where they are

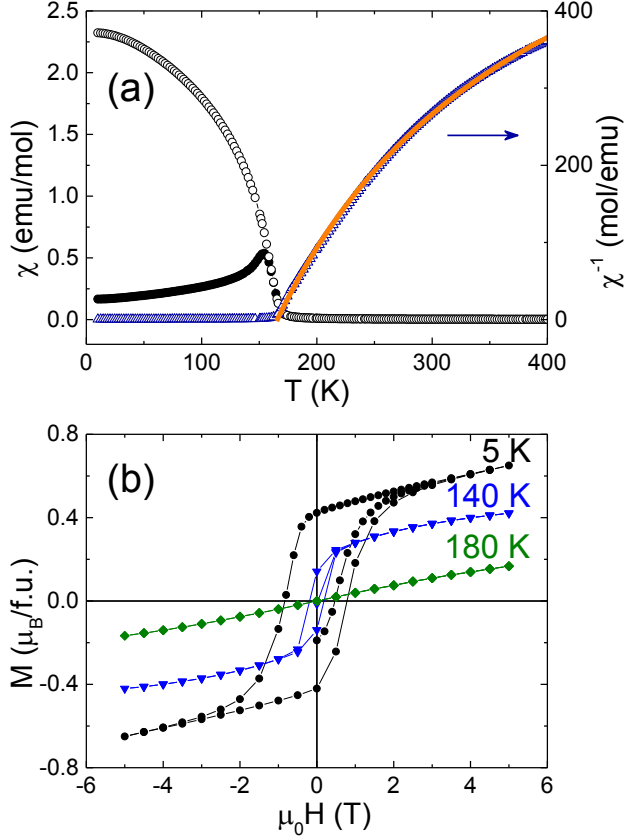perpendicular to the directions of all spin chains, as shown in Figure 3c.

Figure 2. (a) Magnetic susceptibility of V_2OPO_4 as a function of temperature measured in a field of 1000 Oe (closed and open symbols for ZFC and FC respectively) and inverse ZFC magnetic susceptibility (right axis, blue symbols) with the fit (orange line) described in the text. (b) Magnetization-field loops at several temperatures.

The ferrimagnetic order of V^{2+} ($3d^3$) spin up and V^{3+} ($3d^2$) spin down states gives a predicted magnetization of 1 μ_B per formula unit, in fair agreement with the 0.6 μ_B experimental value at 5 K (Figure 2b). However, the saturated V^{2+} and V^{3+} sublattice moments are reduced from ideal values of 3 and 2 μ_B to 1.8(6) and 1.5(6) μ_B. Although the antiferromagnetic coupling between neighboring cations within the chains is consistent with predicted superexchange rule [23], the reduction of ordered moments below T_C and the paramagnetic effective moment above T_C also evidences some direct V-V bonding interactions.

Variable temperature structural studies. Structure refinements against NPD data showed that the monoclinic charge ordered structure persists down to 10 K. The monoclinic lattice parameters (Table S1) do not evidence any structural transition at T_C = 164 K but a small anomaly in the β angle may evidence a slight magnetostriction.

Synchrotron powder X-ray diffraction data collected from 300 up to 750 K show a change in peak splittings and intensities at 605 K (Figures 4 and S2), in agreement with the phase transition around 593 K reported previously [12]. Structure refinements revealed that the structure changes from monoclinic $C2/c$ to tetragonal $I4_1/amd$ at 605 K. Temperature varia-

tions of the refined lattice parameters are shown in Figure 5 using the pseudo-tetragonal setting of the monoclinic cell (monoclinic parameters are in Figure S1).
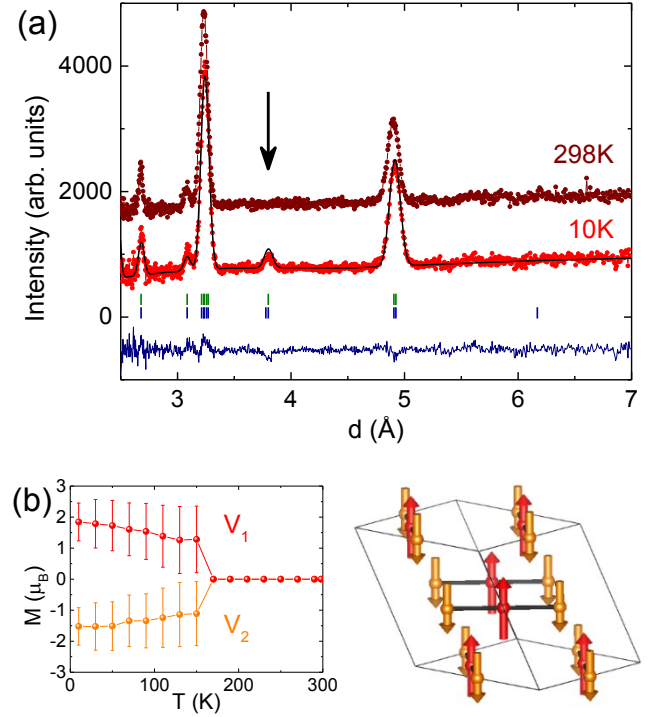

Figure 3. (a) Fits to powder neutron diffraction profiles from the low angle bank on HRPD neutron pattern at 10 and 298 K, with Bragg markers for nuclear (upper) and magnetic (lower) peaks and the difference curve for the 10 K fit also shown. The prominent magnetic intensity at $d \approx 3.8$ Å is arrowed. (b) (right) Magnetic structure of V_2OPO_4 at 10 K with V1(V^{2+}) spins in red and V2 (V^{3+}) in orange, and black lines showing the spin chains; (left) Thermal evolution of the magnetic moments.

The high temperature tetragonal $I4_1/amd$ structure has only one unique V site with an average $V^{2.5+}$ oxidation state. Hence the monoclinic to tetragonal structural transition corresponds to the long range charge ordering transition at T_{CO} = 605 K. This is confirmed by the thermal variations of interpolated BVS in Figure 6 where a critical variation in the difference in charge states is seen from ~500 K up to T_{CO}. The monoclinic distortion angles α_T and γ_T show a similar variation in Figure 5.

The pseudo-tetragonal cell lengths a_T and c_T show a normal positive thermal expansion (PTE) throughout the monoclinic regime as shown in Figure 5. The transition from monoclinic to tetragonal phases appears to be continuous (or quasi-continuous) as no cell volume anomaly or phase coexistence is observed at T_{CO}. However a_T shows a dramatic change of slope to negative thermal expansion (NTE) above T_{CO} and this leads to an overall NTE of the lattice volume. Thermal expansion coefficients defined as $\alpha_p = \Delta p/(p\Delta T)$ for lattice parameters p are plotted in the lower panel of Figure 5. α_V reaches -13.3 x 10^{-6} K^{-1} at 750 K and has an average value of - 5.8 x 10^{-6} K^{-1} in the 620-750 K range, comparable to values in other NTE materials [3,24]. Additional datasets collected while cooling from 750 K confirm the reversibility of the structural transition and the PTE to NTE changeover (Figure S3). The

switch from PTE to NTE at the 605 K charge ordering transition is driven by a switch in the thermal expansion behavior of the $a_T = b_T$ cell parameters, which correspond to the directions of face-sharing chains of VO_6 octahedra. Charge ordering is not in itself expected to drive such a change, but may do so if it also leads to changes in V-V bonding in the chains.
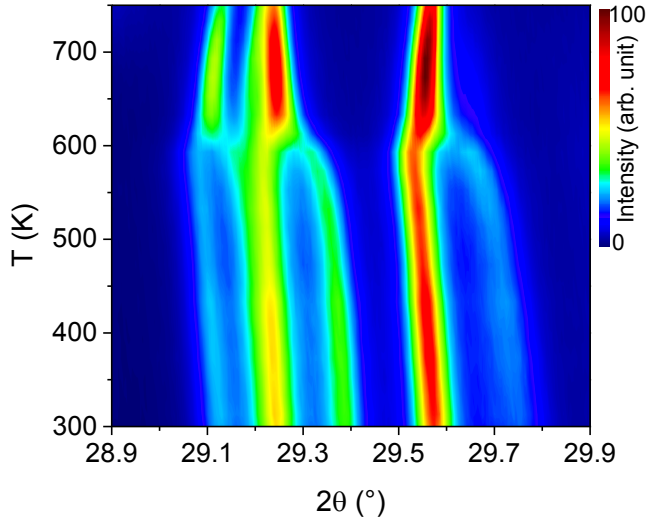

Figure 4. Temperature evolution of a section of the synchrotron X-ray diffraction intensities showing the monoclinic to tetragonal transition at 605 K.

V_2OPO_4 is an insulating framework material so the NTE above T_{CO} is likely to result from large-amplitude transverse vibrations or torsions, as found in many other framework materials [1]. An increase in amplitude of transverse vibrations of the face-bridging oxygens with temperature would decrease the V-O-V angle and shorten the V-V distance along the chain (shown schematically in the Abstract figure). Accurate oxygen temperature factors are not available from our present synchrotron X-ray refinements, and further neutron scattering experiments will be needed to evidence the expected changes in vibrational motion around the transition.

The change to PTE behavior of the a_T parameter and hence lattice volume below T_{CO} implies a change in bonding. Given the short metal-metal distances, this is most likely an onset of V-V bonding in the chains associated with the charge order. The observed ferrimagnetic order below $T_C = 164$ K is consistent with such bonding through pairing of opposing spin t_{2g} electrons on neighboring V^{2+} and V^{3+} cations. Local ferrimagnetic correlations above T_C are evidenced by the large constant contribution χ_0 to the magnetic susceptibility, and these may be associated with V-V bonding that persists up to T_{CO} and is gradually lost on heating through the critical region above T_{CO} as local charge ordering correlations diminish. V-V distances within the chains remain uniform below T_{CO} so the V atoms form an orbital polymer chain rather than discrete orbital molecules such as the dimers observed in VO_2 [21]. Hence the switch from PTE to NTE on warming through the 605 K charge ordering transition is likely due to loss of V-V bonding that enable transverse oxygen motions to dominate the thermal expansion.

Resistivity measurements. The high temperature resistivity (Figure 7) displays a change of slope near 600 K, coinciding

with the structural transition at T_{CO}. V_2OPO_4 is semiconducting below and above the transition, and Arrhenius fits in the 350-450 K and 620-870 K regions give activation energies of 300 and 400 meV respectively. This demonstrates that loss of long charge ordering does not lead to metallization, but instead T_{CO} marks an order to disorder transition of localized V^{2+} and V^{3+} states.
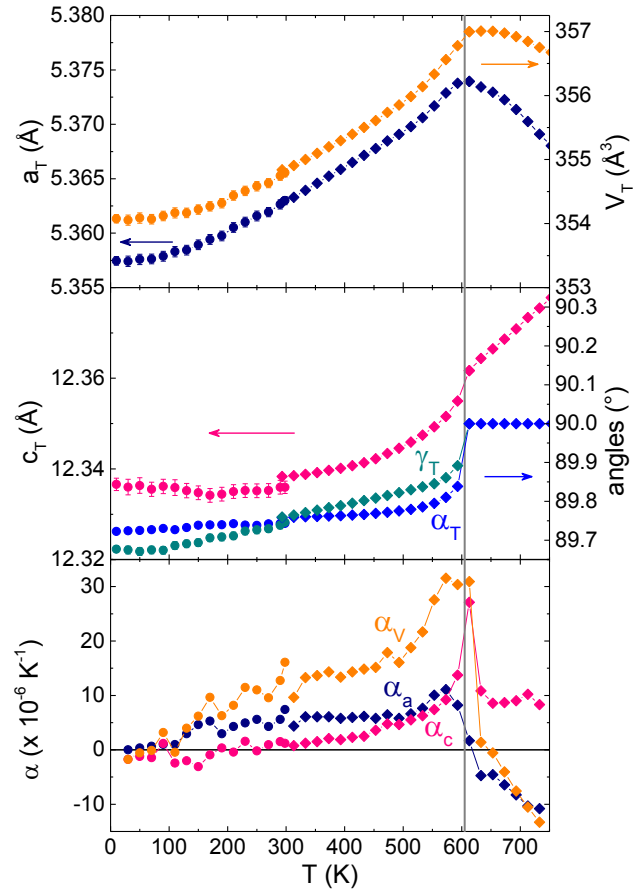

Figure 5. Pseudo-tetragonal unit cell parameters through the $C2/c$ to $I4_1/amd$ transition at 605 K from NPD (circle symbols) and XRD (diamond symbols) and thermal expansion coefficients calculated for the pseudo tetragonal cell.
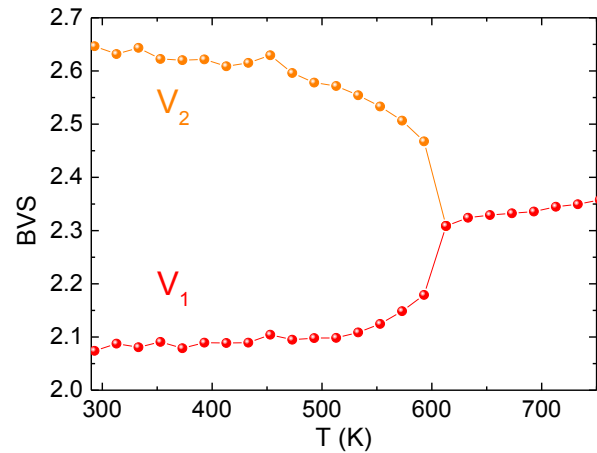

Figure 6. Interpolated Bond Valence Sums for the vanadium cations showing the charge ordering transition.

We also attempted to measure the low temperature resistivity of V_2OPO_4 below room temperature, but the sample resistance was too large to be measured accurately below 205 K. The fitted activation energy between 218 and 300 K of 310 meV, is in good agreement with the value obtained in the 350-450 K region of the charge ordered regime.

Electronic Structure Calculations. Due to the inherent problems associated with calculating paramagnetic states in strongly-correlated materials using standard DFT methods, magnetically ordered calculations were performed for both the monoclinic and tetragonal models, using the experimental unit cells. An on-site Coulomb repulsion term U = 3.5 eV, comparable to values used for V_2O_3 which also contains face-sharing VO_6 octahedra [25,26], was used to treat the correlation of V(d) states in calculating the density of states in Figure 8. The experimentally observed monoclinic magnetic model is found to be lowest in energy. The calculated thermal band gap energy of 420 meV is comparable to the above experimental values of 300-310 meV. Projected magnetic moments (from Mulliken analysis [27,28,29]) are 3.04 μ_B and -2.07 μ_B for V1 (V^{2+}) and V2 (V^{3+}), respectively, and calculated d-orbital populations are 3.48 and 3.19. The large difference between spin and charge suggests some degree of spin polarized charge transfer between V1 and V2 of the majority spin component.
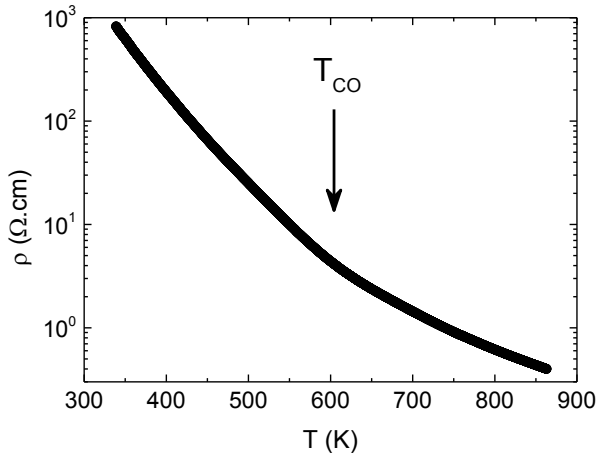

Figure 7. High temperature resistivity showing a change of slope at T_{CO} = 605 K.

For the tetragonal model, calculations were less stable, and different magnetic states had more similar energies. The observed (low temperature) magnetic structure gives a semivalent ground state with a small density of states at the fermi level (Figures 8 and S4). Hence, the calculations predict the lowest energy ground states to be the observed charge-ordered model in the monoclinic structure with ferrimagnetic spin order, but a semivalent metallic state is favored for the tetragonal case (Table S2). This does not agree with the observation of a semiconductivity above T_{CO}, but the discrepancy is understandable as the DFT calculation does not allow for the possibility of a localized but disordered V^{2+}/V^{3+} charge state, or for paramagnetism as noted before.
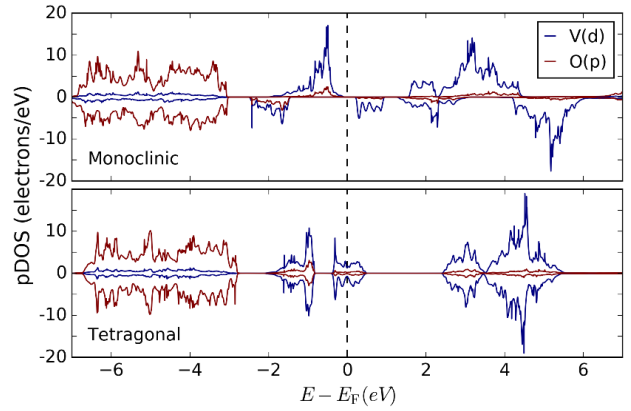

Figure 8. Partial density of states for vanadium d and oxygen p states near Fermi level (E_F) for the charge-order monoclinic and the semi-valent tetragonal phases.

The valence band of the monoclinic phase is dominated by almost dispersionless vanadium d-states (Figure S5). Figure 9a shows a cut through the real-space electron density of the highest occupied band (HOMO), as a weighted sum across reciprocal space. Ideally this corresponds to the majority spin t_{2g} states of the V1 (V^{2+}) sites, but some valence electron transfer to the V2 site is evident. In contrast, the equivalent band representation for the tetragonal semivalent ground state (Figure 9b) shows no electron transfer to between V-sites. This supports the above proposal that weak V-V bonding results from the charge ordering in the monoclinic phase, and drives the change from NTE to PTE behavior on cooling below T_{CO}.
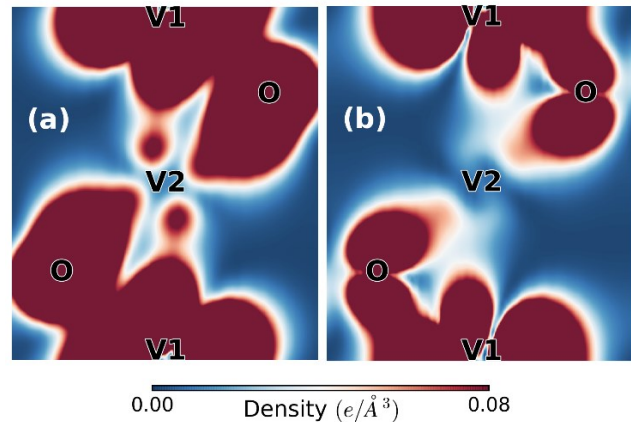

Figure 9. Electron density sections through the highest occupied (HOMO) bands shown on a linear density scale in the 0 - 0.08 electrons.Å^{-3} range. The slice is taken through the (20$\bar{1}$) plane of the primitive cell (equivalent to monoclinic (22$\bar{1}$) and tetragonal (200) planes) and contains a V chain and the interchain bridging oxygen O2. (a) Monoclinic charge-ordered structure showing transfer of charge density from V1 (V^{2+}) to V2 (V^{3+}) sites. (b) Tetragonal semivalent band structure showing no V-V charge transfer. V1 and V2 labels are for comparison purposes, and correspond to crystallographically identical sites in the tetragonal phase.

CONCLUSION

This study has characterized changes of electronic, magnetic, and lattice properties of V_2OPO_4 at two transitions. Long range V^{2+}/V^{3+} charge ordering is observed up to T_{CO} = 605 K

where a monoclinic to tetragonal structural transition and a switch from positive to negative thermal expansion are observed. V-V bonding within orbital polymer chains is proposed as the key factor in the novel switch of thermal expansion behavior, and is consistent with band structure calculations. Ferrimagnetic order of V^{2+} spin up and V^{3+} $(3d^2)$ spin down states is observed below T_C = 164 K, and magnetic susceptibility measurements evidence local spin pairing correlations to higher temperatures. Hence, the combination of active charge, orbital and spin degrees of freedom in V_2OPO_4 is shown to give rise to low temperature ferrimagnetism and a new mechanism for switching between positive and negative volume expansion.

ASSOCIATED CONTENT

Supporting Information. Further structural results, electronic structure calculation results, and irreducible representations for V spins in the magnetically ordered structure. This material is available free of charge via the Internet at http://pubs.acs.org.

AUTHOR INFORMATION

Corresponding Author

* j.p.attfield@ed.ac.uk

Author Contributions

The manuscript was written through contributions of all authors.

Notes

The authors declare no competing financial interest.

ACKNOWLEDGMENT

REFERENCES

(1) Chen, J.; Hu, L.; Deng, J.; Xing, X. *Chem. Soc. Rev.* **2015**, *44*, 3522-3567.

(2) Mary, T. A., Evans, J. S. O., Vogt, T.; Sleight, A. W. Science 1996, *272*, 90–92.

(3) Evans, J. S. O. *J. Chem. Soc., Dalton Trans.* **1999**, 3317-3326.

(4) Greve, B. K.; Martin, K. L.; Lee, P. L.; Chupas, P. J.; Chapman, K. W.; Wilkinson, A. P. *J. Am. Chem. Soc*. **2010**, *132*, 15496–15498.

(5) Attfield, J. P. *Nature* **2011**, *480*, 465–466.

(6) Azuma, M.; Chen, W.-T.; Seki, H.; Czapski, M.; Smirnova, O.; Oka, K.; Mizumaki, M.; Watanuki, T.; Ishimatsu, N.; Kawamura, N.; Ishiwata, S.; Tucker, M. G.; Shimakawa, Y.; Attfield, J. P. *Nature Commun*. **2011**, 2, 347.

(7) Attfield, J. P. *APL Mater.* **2015**, *3,* 041510.

(8) Kajita, T.; Kanzaki, T.; Suzuki, T.; Kim, J. E.; Kato, K.; Takata, M.; Katsufuji, T. *Phys. Rev. B* **2010**, *81,* 060405(R).

(9) Takubo, K.; Kanzaki, T.; Yamasaki, Y.; Nakao, H.; Murakami, Y.; Oguchi, T.; Katsufuji, T. *Phys. Rev. B* **2012**, *86,* 085141.

(10) Bridges, C. A.; Greedan, J. E.; Kleinke, H. *J. Solid State Chem.* **2004**, *177,* 4516-4527.

(11) Horibe, Y.; Shingu, M.; Kurushima, K.; Ishibashi, H.; Ikeda, N.; Kato, K.; Motome, Y.; Furukawa, N.; Mori, S.; Katsufuji, T. *Phys. Rev. Lett.* **2006,** *96,* 086406.

(12) Glaum, R.; Gruehn, R. *Z. Kristallogr.* **1989**, *186,* 91-93.

(13) Bordes. E.; Courtine, P. *J. Catal.* **1979**, *57,* 236-252.

(14) Rodriguez-Carvajal, J. *Physica B* **1993**, *192,* 55-69.

(15) Clark, S. J.; Segall, M. D.; Pickard, C. J.; Hasnip, P. J.; Probert, M. J.; Refson, K.; Payne, M. C. *Z. Kristallogr.* **2005**, *220,* 567-570.

(16) Monkhorst, H.J.; Pack, J.D. *Phys. Rev. B* **1976**, *13,* 5188-5192.

(17) Morris, A. J.; Nicholls, R. J.; Pickard, C. J.; Yates, J. R. *Comput. Phys. Commun.* **2014**, *185,* 1477-1485.

(18) Yates, J. R.; Wang, X.; Vanderbilt, D.; Souza, I. *Phys. Rev. B* **2007**, *75,* 195121.

(19) Elkaïm, E.; Berar, J. F.; Gleitzer, C.; Malaman, B.; Ijjaali, M.; Lecomte, C. *Acta Cryst. B* **1996**, *52,* 428-431.

(20) Stephens, P. W. *J. Appl. Cryst.* **1999**, *32,* 281-289.

(21) Rogers, D. B.; Shannon, R. D.; Sleight, A. W.; Gillson, J. L. *Inorg. Chem.* **1969**, *8,* 841-849.

(22) Attfield, J. P. *Solid State Sci.* **2006**, *8,* 861-867.

(23) Goodenough, J. B. *Phys. Rev.* **1960**, *117,* 1442-1451.

(24) Miller, W.; Smith, C. W.; Mackenzie, D. S.; Evans, K. E. *J. Mater Sci.* **2009**, *44,* 5441-5451.

(25) Lo Vecchio, I.; Denlinger, J. D.; Krupin, O.; Kim, B. J.; Metcalf, P. A.; Lupi, S.; Allen, J. W.; Lanzara, A. *Phys. Rev. Lett.* **2016**, *117,* 166401.

(26) Grieger, D.; Fabrizio, M. *Phys. Rev. B* **2015**, *92,* 075121.

(27) Mulliken, R. S. *J. Chem. Phys.* **1955**, *23,* 1833-1840.

(28) Segall, M. D.; Pickard, C. J.; Shah, R.; Payne, M. C. *Mol. Phys.* **1996**, *89,* 571-577.

(29) Segall, M. D.; Shah, R.; Pickard, C. J.; Payne, M. C. *Phys. Rev. B* **1996**, *54,* 16317-16320.

TOC graphic